INTERNATIONAL JOURNAL FOR NUMERICAL METHODS IN ENGINEERING
Int. J. Numer. Meth. Engng 2009; **77**:702–718
Published online 15 August 2008 in Wiley InterScience (www.interscience.wiley.com). DOI: 10.1002/nme.2433

An efficient numerical method for solid–liquid transitions in optical rewritable recording

J. H. Brusche[1], A. Segal[1] and C. Vuik[2,*,†]

[1]*Delft Institute of Applied Mathematics, Delft University of Technology, Delft, Netherlands*
[2]*TU Delft, DIAM, Delft, Netherlands*

SUMMARY

Melting and solidification processes are encountered in a variety of industrial applications. Examples include the steel industry, food processing and the recording of data in optical data storage. The phase transition, induced by a heat source, can be described by a two-phase Stefan formulation. To solve such highly non-linear moving boundary problems within industrially relevant domains, we propose an extension to 3D space of the temperature-based method described by Fachinotti *et al*. (*Int. J. Numer. Meth. Engng* 1999; **44**(12):1863–1884). By the use of discontinuous spatial integration accurate solutions can be efficiently obtained for isothermal problems that are driven by the boundary conditions. However, the temperature approach can fail for isothermal problems that are driven by an (external) source. This is remedied by introducing an artificial mushy region around the melting temperature. The developed method has been applied to 3D optical rewritable recording simulations. Copyright © 2008 John Wiley & Sons, Ltd.

Received 1 February 2008; Revised 24 June 2008; Accepted 24 June 2008

KEY WORDS: solid–liquid transition; enthalpy; finite element method

1. INTRODUCTION

Processes involving solid–liquid phase-change phenomena are commonly encountered in industrial applications [1, 2]. Depending on the composition of the material, melting occurs either at a melting *point* T_m or along a melting *trajectory*. In case the phase change occurs at a melting point, the interface between the solid and the liquid phase is *sharp*. These so-called isothermal problems can be described as a two-phase Stefan problem. For a non-isothermal problem, a so-called *mushy region*, which can be characterized by solids suspended in a liquid region, separates the solid and the liquid phase.

*Correspondence to: C. Vuik, TU Delft, DIAM, Delft, Netherlands.
†E-mail: c.vuik@math.tudelft.nl

Contract/grant sponsor: Dutch Technology Foundation (STW)

An important characteristic of phase-change problems arising from industrial applications is that the domain of interest consists of a complex 3D geometry, which in addition can be composed of various subdomains containing different materials. A typical application in which phase-change phenomena occur within a complex composite structure is the writing process in optical rewritable recording. Optical rewritable discs contain one or more so-called recording stacks. These stacks consist of various grooved layers. At least one of these layers consists of a so-called phase-change material. In this layer, amorphous regions (*marks*) are formed on a crystalline background by means of high-power laser pulses. During read-out, differences in reflectivity of the amorphous and crystalline material can be detected and converted into a binary data string. The final shape and size of an amorphous mark are determined by the region that melts due to the absorbed laser light and recrystallization at the melting front.

The often complex composition of the computational domain makes that the choice of a numerical method for solving general solid–liquid transition problems inside these domains is limited. A suitable method should also be capable of dealing with multiple separate fronts and has to allow for merging and breaking of these fronts. Finally, in order to be feasible for industrial applications, the method is preferably simple (implementation/comprehension) and efficient (memory/computational time).

In the literature on solving phase-change problems, various *fixed-grid* methods have been proposed for isothermal as well as mushy problems. These methods consider either an enthalpy [3] or a temperature formulation [4] of the energy conservation equation. In the enthalpy formulation, in which the enthalpy and temperature are the unknowns, the change of enthalpy is described by a single energy balance equation. This equation holds across the whole domain of interest. Because the latent heat is implicitly accounted for in the enthalpy, the phase-change front is not actively tracked, but can be derived later from the calculated temperatures. In the temperature formulation, the temperature is the single dependent variable. The inclusion of latent heat is accounted for by an additional non-linear term that is included into the classical heat diffusion equation.

In general, the enthalpy-based methods perform best in the case of non-isothermal problems. For isothermal problems, the enthalpy approach suffers from an inherent drawback: the computed temperatures at a given point in the domain show a step-like behavior (*staircasing*) [3, 5]. A smoothing of the enthalpy function [6], a relaxed linearization of the enthalpy [7], or a refinement of the mesh [5] can be employed. These approaches can only reduce the staircasing to some extent. Numerical schemes have been proposed to remove these oscillations, see, for instance, Chun and Park [8] or Date [9]. However, these techniques require either temperature constraints or suitable time integration schemes to keep track of the moving front, thus undermining the inherent advantage of the enthalpy formulation. Moreover, these methods are cumbersome to implement in higher dimensions with multiple phase fronts.

In the case of composite domains containing different materials, the enthalpy-based methods suffer from a second drawback: the enthalpy will jump at the interface between adjacent layers. Alexiades and Solomon [10] illustrate how the enthalpy method can be applied in the case of a 1D slab consisting of two layers. Their strategy is to consider the interface between the two different layers as an interface that moves at zero speed. The solution can then efficiently be found using, for instance, the Elliot–Ockendon SOR method [11]. In higher spatial dimensions, however, it becomes increasingly more challenging in case the fixed interfaces are non-planar.

A distinctive feature of the temperature-based methods for *fixed grids* is the application of discontinuous spatial integration. The key idea behind discontinuous integration [4] is that for each element of the finite element mesh that is occupied by more than one phase of the phase-change

DOI: 10.1002/nme

material, all the integrals over the element are computed as the combination of the integral contributions over the subdomains separately.

We extended the temperature method of Fachinotti *et al*. [12] to 3D problems. In addition, the developed numerical method is modified such that it can be used to solve phase transition problems for complex composite domains that are driven by a heat source. The method has been developed to accurately model the melting component of the mark formation process in optical rewritable recording. However, the presented method can be easily used to model phase transition problems arising from various other industrial applications.

In contrast to Fachinotti *et al*. and other authors, instead of Gauss quadratures or integral evaluation in closed analytical form, we prefer the use of simple Newton–Cotes integration. Euler backward time integration is employed, so that the only restriction on the time step size is enforced based on the change in the position of the advancing front during a time step, which may not skip elements. This can be interpreted as a Courant–Friedrichs–Lewy-type condition. The Newton–Raphson iteration procedure is used to solve the non-linear system in an efficient way. To improve global convergence, in particular in the case of larger values of the latent heat, a line search algorithm is added. The (eventual) quadratic convergence rate makes that the temperature approach can be very cost efficient.

The structure of this paper is as follows. In Section 2 a moving boundary formulation of the melting problem is given. The temperature method and its extension to 3D are described in Section 3. The discontinuous spatial integration technique, the time discretization and the solution of the non-linear discrete system of equations are discussed. In particular, the numerical challenges that arise in the case of isothermal problems that are driven by a heat source are addressed. As a remedy to overcome these difficulties, the introduction of an artificial mushy region is proposed in Section 4. In the Section 5, several results are presented for Blu-ray recording simulations. Conclusions are drawn in Section 6.

2. PROBLEM DEFINITION

Let Ω be a prescribed subdomain of $\mathbb{R}^n$ with a fixed outer boundary $\delta\Omega$, see Figure 1. The domain Ω consists of one or more disjunct, possibly composite, subdomains, each containing a different material. At least one of these subdomains, Ω_{pc}, consists of a material that will undergo a change of phase due to a heat source $Q(\mathbf{x}, t)$. At any given time t, the temperature $T(\mathbf{x}, t)$ in the computational domain Ω satisfies the following governing equation:

$$\rho c(T)\frac{\partial T}{\partial t}+\rho\mathscr{L}\frac{\partial f_{\mathrm{l}}}{\partial t}-\nabla\cdot(\kappa(T)\nabla T)=Q \tag{1}$$

where c is the heat capacity, $\mathscr{L}$ the latent heat, and κ the thermal conductivity. The density ρ is assumed to be the same constant in the liquid and the solid phase. Because of the composition of Ω, except for ρ, each of these coefficients depends on position and time. In Ω_{pc}, the change of phase is described by the liquid volume fraction f_{l} (f_{l} is assumed to be zero in $\Omega\backslash\Omega_{\mathrm{pc}}$). From a certain time t_{m}, $t_0\leqslant t_{\mathrm{m}}\leqslant t_{\mathrm{end}}$, Ω_{pc} is composed of two disjunct, possibly composite, subdomains $\Omega_{\mathrm{s}}(t)$ and $\Omega_{\mathrm{l}}(t)$, occupied by the solid and liquid phases of the phase-change material, respectively. For pure materials, the phase change occurs at a melting point T_{m}. In this case, the subdomains $\Omega_{\mathrm{s}}(t)$ and $\Omega_{\mathrm{l}}(t)$ are separated by a *sharp* moving boundary $\Gamma(t)$ and f_{l} is taken equal to the Heavyside step

DOI: 10.1002/nme

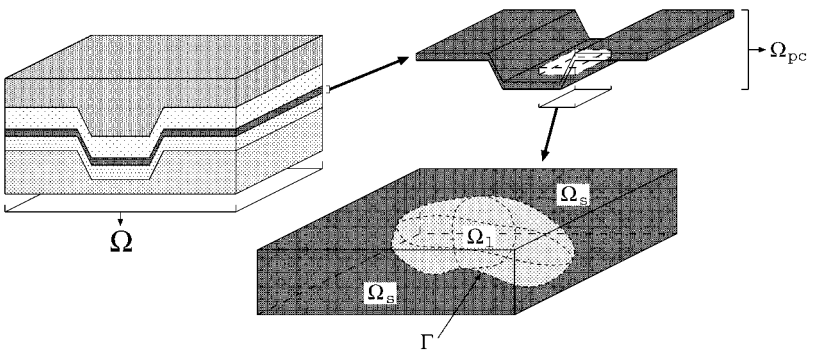

Figure 1. The computational domain Ω, the phase-change layer Ω_{pc} and the solid and liquid subdomains $\Omega_s(t)$ and $\Omega_l(t)$, respectively.

function $\mathscr{H}(T-T_m)$. In the case of a mushy phase transition, f_l is given as

$$f_l = \begin{cases} 0, & T \leqslant T_s \\ 0 < f^*(T) \leqslant 1, & T_s < T \leqslant T_l \\ 1, & T > T_l \end{cases} \tag{2}$$

where the mushy region is bounded by the solidification temperature T_s and liquification temperature T_l, and $f^*(T)$ is a continuous function that represents the transition trajectory. Note that in the above temperature formulation no explicit Stefan conditions are imposed at the phase boundaries.

The governing equation (1) is supplemented by the initial condition

$$T(\mathbf{x}, t_0) = \bar{T}(\mathbf{x}) \quad \text{for all } \mathbf{x} \in \Omega \tag{3}$$

and appropriate boundary conditions on the fixed outer boundary $\delta\Omega$. It is assumed that at $t = t_0$, the whole domain Ω is solid.

3. METHOD DESCRIPTION

Without the presence of a moving phase front, Equation (1) reduces to the classic heat diffusion equation. Therefore, a finite element discretization [13] of Equation (1) is straightforward, except for elements that are occupied by more than one phase. In Ω the temperature field is approximated by

$$T(\mathbf{x}, t) \approx \hat{T}(\mathbf{x}, t) = \sum_{i=1}^{n} \phi_i(\mathbf{x}) T_i(t) \tag{4}$$

where ϕ_i is a basis function and T_i the nodal temperature. The application of the general Galerkin procedure, in which the weighting functions are taken to be equal to the basis functions, leads to the following semi-discrete weak formulation:

$$\mathbf{M}\frac{\mathrm{d}\mathbf{T}}{\mathrm{d}t} + \frac{\mathrm{d}\mathbf{L}}{\mathrm{d}t} + \mathbf{S}\mathbf{T} = \mathbf{Q} \tag{5}$$

DOI: 10.1002/nme

The entries of the mass matrix **M**, stiffness matrix **S**, latent heat vector **L**, and heat source vector **Q** are given as (boundary conditions have been omitted)

$$M_{ij} = \int_\Omega \rho c \phi_i \phi_j \, \mathrm{d}\Omega \tag{6}$$

$$S_{ij} = \int_\Omega \nabla \phi_i \cdot (\kappa \nabla \phi_j) \, \mathrm{d}\Omega \tag{7}$$

$$L_i = \int_\Omega \rho \mathscr{L} \phi_i f_\mathrm{l} \, \mathrm{d}\Omega \tag{8}$$

$$Q_i = \int_\Omega \phi_i Q \, \mathrm{d}\Omega \tag{9}$$

The distinctive feature of the temperature-based approach is the use of discontinuous integration in space. The key idea behind discontinuous integration, as, for instance, described by Fachinotti *et al.* [12] and references therein, is that for elements intersected by a phase boundary, the integrals (6)–(9) are not computed over an element as a whole, using, for instance, averaged values for the physical parameters, but are instead computed over the one-phase subdomains separately. That is, in, for example, the isothermal case as illustrated in Figure 2, the (i, j)th entry of the element mass matrix of the intersected element e with volume Ω^e is computed as

$$M_{ij} = \int_{\Omega^e} \rho c \phi_i \phi_j \, \mathrm{d}\Omega = \int_{\Omega_s^e} \rho_s c_s \phi_i \phi_j \, \mathrm{d}\Omega + \int_{\Omega_l^e} \rho_l c_l \phi_i \phi_j \, \mathrm{d}\Omega \tag{10}$$

3.1. Spatial integration

In Reference [12], discontinuous integration is applied to solve 2D heat diffusion problems involving a phase transition. Fachinotti and coauthors propose the use of analytical integration and linear triangular elements. They claim that in this way the efficiency of the integration process considerably improves when compared with the use of Gaussian quadrature, see, for instance, Crivelli *et al.* [4], because their analytical approach requires neither extra mappings nor a summation over sample points.

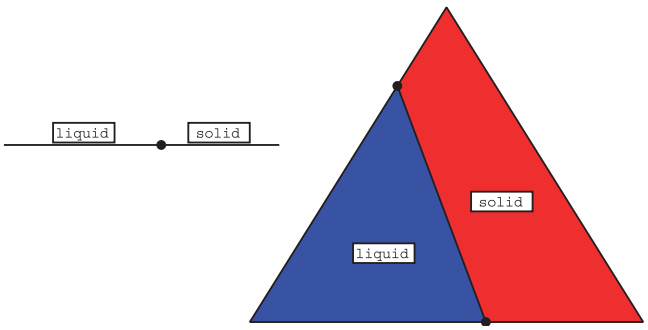

Figure 2. For isothermal phase change the intersection of simplices in 1D and 2D is almost trivial.

DOI: 10.1002/nme

However, despite of what is stated by Fachinotti *et al*., we consider the use of a Newton–Cotes numerical integration rule to be a more practical choice. Firstly, only a (weighted) summation over sample points is required. Secondly, the proposed analytical method by Fachinotti *et al*. does require several matrix–vector/matrix–matrix products and matrix inversions. Although the dimensions of these matrices and vectors are small, the mappings are more costly than a simple summation over sample points. Lastly, when Newton–Cotes integration is applied, there is no restriction on the coefficients of being constants for each phase.

Because the solution to Equation (1), in presence of a melting front, will in general not be smooth near this front, linear elements are used. The points at which the edges of the simplex are intersected by an isosurface, along which the temperature is either equal to T_{m} (in case of isothermal phase change), or T_{s} or T_{l} (in case of isothermal phase change), are found by means of linear interpolation. These intersection points are connected by straight line segments, which result in a linear approximation of the boundary surface segment inside the element. This approximation is another motivation for choosing linear basis functions.

As a result of these choices, in 2D at least one of the one-phase subdomains of an intersected element is once again a linear subtriangle, see Figure 2. Thus, the computation of, for example, M_{ij}, cf. (10), comes down to the evaluation of an integral over a triangular subelement and a remainder. Let us assume that the triangular subdomain is occupied by the liquid phase and the remainder by the solid phase. The integral over the triangular subdomain is computed using a Newton–Cotes rule. The integral contribution for the remainder can be computed in two ways, see Figure 3.

(I) The remainder is subdivided into triangular subelements and the contributions are coherently summed up.
(II) The integral over the remainder is obtained by first evaluating the integral over the whole element as if it was fully occupied by the solid phase and then subtracting the contribution over the triangular subdomain for the same phase.

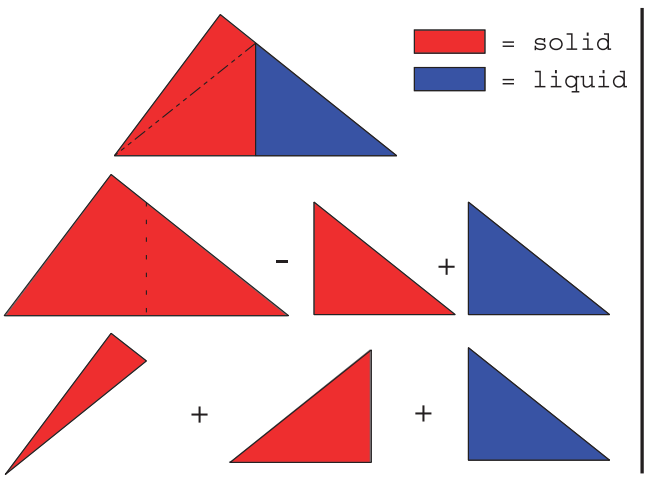

Figure 3. Two ways of computing the integrals over the one-phase subdomains of a 2D linear triangular element.

DOI: 10.1002/nme

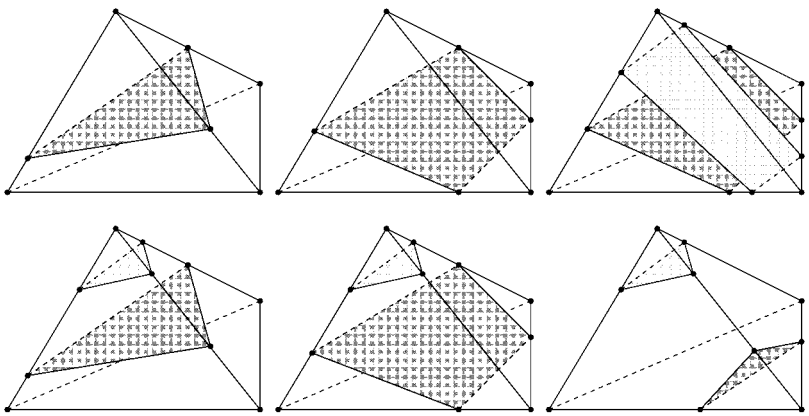

Figure 4. In the case of mushy phase transition, six geometrically different intersections with the T_s and T_l isosurfaces are possible in 3D.

The same principles can be used for mushy phase transitions, in which case an element can be separated into any combination of a solid, liquid, and mushy subdomain.

In 3D, the intersection of a linear tetrahedron by a phase front is either a triangle or a quadrilateral. In the case of mushy phase change, six geometrically different intersections are possible, as illustrated in Figure 4. When the phase boundary segment is triangular, the integrals over the trapezoidal subdomain can be computed using a 3D equivalent of either method I or method II. When the phase boundary segment is a quadrilateral, of which in general the vertices do not lie in a plane, only a subdivision into six tetrahedra is feasible. This subdivision also determines how the quadrilateral is divided into two linear triangles. However, any error that is introduced in this way is of the same order as that of the approximations with the linear elements.

3.2. Time discretization

In order to obtain a fully discretized system of equations, the time derivatives in (1) are approximated by means of Euler backward discretization. That is, at time level $m+1$,

$$\mathbf{\Psi}(\mathbf{T}^{m+1}) = \mathbf{M}^{m+1}\frac{\mathbf{T}^{m+1}-\mathbf{T}^{m}}{\Delta t} + \frac{\mathbf{L}^{m+1}-\mathbf{L}^{m}}{\Delta t} + \mathbf{S}^{m+1}\mathbf{T}^{m+1} - \mathbf{Q}^{m+1} = \mathbf{0} \tag{11}$$

where the mass matrix $\mathbf{M}^{m+1}$ and the stiffness matrix $\mathbf{S}^{m+1}$ are functions of the temperature distribution $\mathbf{T}^{m+1}$. Although the Euler backward discretization is only first-order accurate in time and the resulting system (11) is implicit, the main advantage is that it is unconditionally stable. The Crank–Nicolson scheme, which is also unconditionally stable, is prone to oscillations when the time step is not small enough. Moreover, in particular for isothermal problems, second-order accuracy cannot be expected using Crank–Nicolson owing to the latent heat term.

Even though Euler backward discretization is unconditionally stable, the time step is to be taken such that the moving front does not pass over a full element during a time step. This restriction on the time step ensures that any physical phenomenon, such as the latent heat release, is properly taken into account.

DOI: 10.1002/nme

3.3. Solving the non-linear system

In the temperature formulation, the heat diffusion equation (1) is highly nonlinear owing to the presence of the latent heat term $\partial f_l/\partial t$ and the temperature dependence of c and κ. The solution to the corresponding fully discretized system of Equations (11) can be found using a Newton–Raphson iterative procedure. The main advantage of this approach is that locally quadratic convergence can be obtained. Starting with an initial guess $\mathbf{T}_0^{m+1}=\mathbf{T}^m$, the subsequent approximations of the solution $\mathbf{T}_k, k=1,2,\ldots,$ of (11) are computed using

$$\mathbf{T}_k=\mathbf{T}_{k-1}+\Delta\mathbf{T}_{k-1} \tag{12}$$

where ΔT_{k-1} is the solution of the linear system

$$\mathbf{J}(\mathbf{T}_{k-1})\Delta\mathbf{T}_{k-1}=-\Psi(\mathbf{T}_{k-1}) \tag{13}$$

The Jacobian $\mathbf{J}$ is approximated by

$$\mathbf{J}(\mathbf{T}_{k-1})=\frac{\partial\boldsymbol{\Psi}}{\partial\mathbf{T}}=\frac{1}{\Delta t}\left(\mathbf{M}_{k-1}+\frac{\partial\mathbf{L}_{k-1}}{\partial\mathbf{T}}\right)+\mathbf{S}_{k-1} \tag{14}$$

The partial derivative of the latent heat vector $\mathbf{L}$ with respect to the temperature $\mathbf{T}$ needs special attention in case the phase transition is isothermal. Let L_i^e be the ith component of the element vector representing the latent heat release in an element e as defined by (8), Ω^e the volume of e, and Γ^e the segment of the moving boundary contained in e. According to Fachinotti *et al.* [12], each entry (i,j) of the element derivative matrix $\partial L_i^e/\partial T_j$ can be rewritten as an integral over Γ^e

$$\frac{\partial L_i^e}{\partial T_j}=\rho\mathscr{L}\int_{\Omega^e}\delta(\hat{T}-T_{\mathrm{m}})\phi_i\phi_j\,\mathrm{d}\Omega^e=\frac{\rho\mathscr{L}}{\|\nabla T\|}\int_{\Gamma^e}\phi_i\phi_j\,\mathrm{d}\Gamma^e \tag{15}$$

where $\|\nabla T\|$ is the Euclidean norm of the temperature gradient, which is constant on Γ^e due to our choice of basis functions, and δ is the Dirac delta function. Note that the position of the moving interface inside e, which is determined via linear interpolation, is updated for each iteration level k.

In practice, divergence of the Newton–Raphson scheme is often observed in case the latent heat is relatively large in comparison with the other physical parameters. The reason for the non-convergence is that the computed Newton update $\Delta\mathbf{T}_{k-1}$ is too large. Therefore, the Newton update is relaxed using a line search procedure, see, for instance, [14]:

$$\mathbf{T}_k=\mathbf{T}_{k-1}+\alpha\Delta\mathbf{T}_{k-1} \tag{16}$$

where $0<\alpha<1$ is determined by minimizing $\psi=\|\boldsymbol{\Psi}\|_2^2$.

If we define $g(\alpha)\equiv\psi(\mathbf{T}_{k-1}+\alpha\Delta\mathbf{T}_{k-1})$, then $g'(\alpha)=(\nabla\psi)^{\mathrm{T}}\Delta\mathbf{T}_{k-1}$. That is, we have $g(0)$ and $g'(0)$ available (the initial guess). Moreover, a line search is only needed when the full Newton step, i.e. $\alpha=1$, is not acceptable. We then also have $g(1)$ at our disposal. The idea now is to model g as a polynomial $\tilde{g}$ in α and to choose α such that it minimizes the function $\tilde{g}$. This α is found by setting $\tilde{g}'(\alpha)=0$ and then to solve for α.

We propose the use of a quadratic model, $\tilde{g}(\alpha)=a\alpha^2+b\alpha+c$, for all backtracking steps. Starting with $\alpha_1=1$ and $\alpha_2=0$, the coefficients a, b, and c are found using the known values of $g(\alpha_1)$,

DOI: 10.1002/nme

$g(\alpha_2)$, and $g'(\alpha_2)$ given as

$$a = [g(\alpha_1) - g(\alpha_2) + g'(\alpha_2)(\alpha_2 - \alpha_1)]/(\alpha_2 - \alpha_1)^2 \tag{17}$$

$$b = g'(\alpha_2) - 2a\alpha_2 \tag{18}$$

$$c = g(\alpha_2) - g'(\alpha_2)\alpha_2 + a\alpha_2^2 \tag{19}$$

The minimum for this quadratic form is found at

$$\alpha = \alpha_2 - g'(\alpha_2)/2a \tag{20}$$

According to Reference [14], it is advised to require that $0.1\alpha_1 \leqslant \alpha \leqslant 0.5\alpha_1$. Since our aim is to improve the Newton update, in practice a maximum of only 5–10 line search iterations are used to update α.

3.4. The addition of a source term to an isothermal problem

Most test cases found in the literature on Stefan problems consider moving fronts induced by boundary conditions on the fixed boundaries of the computational domain. For these problems, discontinuous integration can be applied without an explicit regularization of the enthalpy function. However, many industrial problems are governed by a source term, and not by boundary conditions on the fixed boundaries. For example, in optical rewritable recording, marks are formed as a result of the absorption of the energy contained in the incident laser light. Moreover, initially there is no moving boundary. New moving fronts appear during the simulation.

In the case of isothermal problems, the use of discontinuous integration cannot prevent that, due to the source term and the moving boundaries that are induced by this source, poor convergence of the Newton–Raphson scheme is observed. The moment that the temperature exceeds T_m in one or more points of the computational domain during the iterative process, the effect of latent heat is taken into account, so that $\partial f_\mathrm{l}/\partial t \neq 0$. As a consequence of the initial overshoot and the jump in the enthalpy, the temperature profile in subsequent iterations exhibits overshoots and undershoots. If the time step size is kept unchanged, the solution will alternate between different states, see Figure 5. A reduction of the time step can prove beneficial, but for increasingly larger values of the latent heat, a breakdown of the iterative procedure is imminent. The introduction of an artificial mushy region can counteract this behavior. The regularization of the enthalpy allows for the approximate solution to lie within a small band around the melting temperature T_m, see

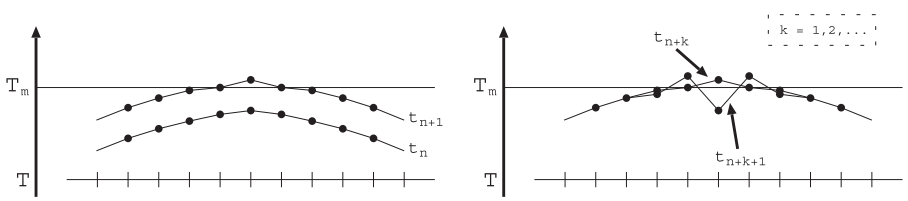

Figure 5. The appearance of two new (source term induced) moving interfaces: evolution of the numerical solution in time. Isothermal case.

DOI: 10.1002/nme

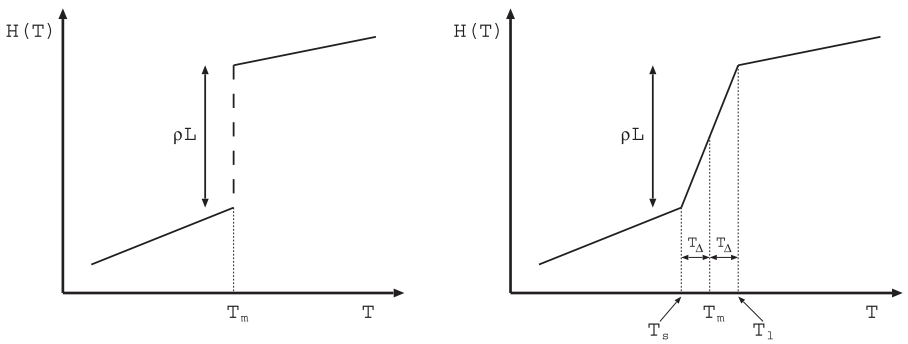

Figure 6. Enthalpy H as function of temperature T. Isothermal case (left) and Artificial mushy region (right).

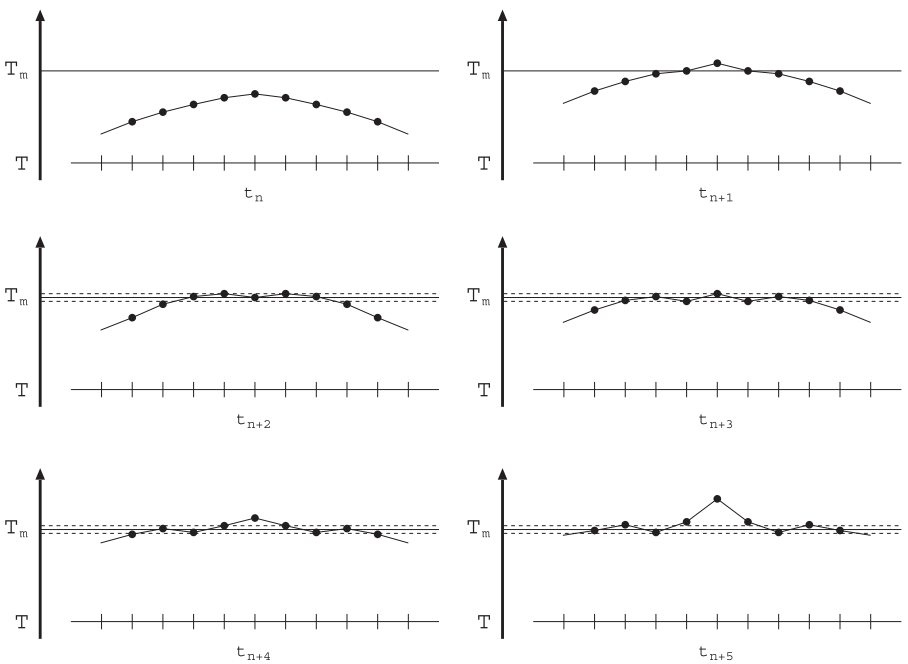

Figure 7. The appearance of two new (source term induced) moving interfaces: evolution of the numerical solution in time using an artificial mushy region.

Figure 6. It suffices to approximate the enthalpy change inside the mushy region, described by $f^*(T)$ in (2), by a linear function

$$f^*(T) = \frac{T - T_\mathrm{s}}{T_\mathrm{l} - T_\mathrm{s}} \tag{21}$$

This choice is feasible because we use linear basis functions and the application of discontinuous integration does not require differentiability of the enthalpy function. The width of the mushy

DOI: 10.1002/nme

region is determined by a mushy parameter T_Δ using

$$T_s = T_m - T_\Delta, \quad T_l = T_m + T_\Delta \tag{22}$$

The effect of the introduction of an artificial mushy region on the evolution in time of the temperature distribution is sketched in Figure 7. As can be seen from the figure, the artificial region allows for minor oscillations of the numerical solution around the melting temperature.

4. NUMERICAL RESULTS

In the previous section it has been explained that the isothermal approach can fail in case a source is added to the problem formulation. This drawback can be overcome by means of introducing an artificial mushy region. A pivotal parameter in this is the width of the mushy zone T_Δ. In this section, we will limit our study to 1D problems. The physical parameters of the test problems considered are taken equal to those used in DVD recording simulations [15]. The values for these parameters are $\kappa_s = \kappa_l = 0.006\,\mathrm{W/cm/^\circ C}$, $\rho c_s = \rho c_l = 12.85\,\mathrm{J/cm^3/^\circ C}$, $L = 6400\,\mathrm{J/kg^\circ C}$ and $T_m = 620^\circ\mathrm{C}$. At $t = 0$, the interval $[-1, 1]\,\mathrm{cm}$ is solid at a temperature of $0^\circ\mathrm{C}$ and the fixed outer boundaries are taken to be isolated. Two Gaussian source functions, $Q_2(x) = 3.5 \times 10^2 \exp(-\frac{1}{2}x^2/\sigma^2)$ and $Q_4(x) = 3.5 \times 10^2 \exp(-\frac{1}{2}x^2/\sigma^4)$, are considered, where the subscripts refer to the power of σ. In our example we choose $\sigma = 1/\sqrt{2\pi}$.

In the case of isothermal problems that are driven by a non-trivial source term, the artificial mushy parameter T_Δ is preferably chosen such that the solution to the regularized problem approximates the non-regularized solution as precise as possible. Note that the choice of T_Δ strongly depends on the application. It is convenient to express T_Δ in terms of a percentage of the melting temperature T_m.

In Table I results are listed for varying T_Δ for a fixed number of elements n and time step Δt. The stopping criterion for the Newton–Raphson iterative process is $\|\boldsymbol{\Psi}(\mathbf{T}_i^{m+1})\|_\infty < \varepsilon \|\boldsymbol{\Psi}(\mathbf{T}^m)\|_\infty$. In this table, as in future tables, x_m denotes the leftmost point at which the moving interface intersects the melting temperature at the final time $t_{end} = 100\,\mathrm{s}$. The abbreviation *#iters* is used to indicate the average number of Newton iterations per time step. The CPU time is given in seconds. Computations have been performed on an Intel Pentium 4 2.4 GHz computer running Linux. The numerical solution is compared with a reference solution $\mathbf{T}_{ref}$, which is numerically obtained on

Table I. The effect of varying the mushy parameter T_Δ (in % of the melting temperature T_m).

	T_Δ	CPU time	#iters	Err_2	Err_∞
$Q_2(x)$	10	7.8	2.4	1.1×10^{-2}	1.9×10^{-2}
	0.1	8.3	4.7	1.2×10^{-3}	3.2×10^{-3}
	0.001	11	9.9	1.2×10^{-3}	3.4×10^{-3}
$Q_4(x)$	10	7.8	2.7	7.4×10^{-3}	7.3×10^{-3}
	0.1	8.4	3.9	2.8×10^{-3}	2.6×10^{-3}
	0.001	8.5	4.9	2.8×10^{-3}	2.7×10^{-3}

$\Delta t = 1\,\mathrm{s}$, $n = 100$, $\varepsilon = 10^{-6}$.

DOI: 10.1002/nme

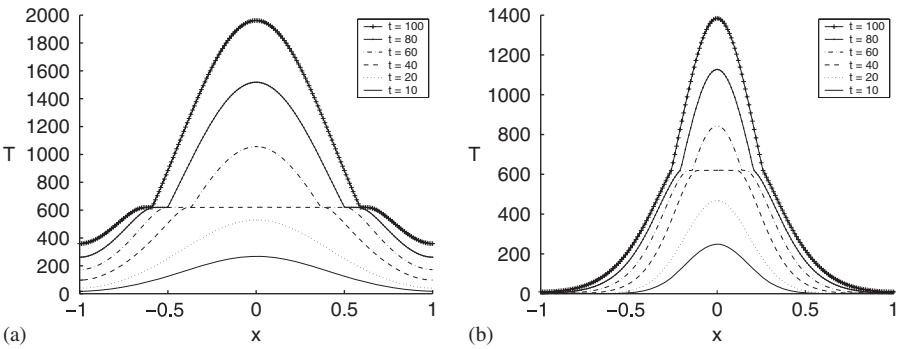

Figure 8. Reference solutions T_{ref}. (a) $Q_2(x) = 3.5 \times 10^2 \exp(-\frac{1}{2}x^2/\sigma^2)$ and (b) $Q_4(x) = 3.5 \times 10^2 \exp(-\frac{1}{2}x^2/\sigma^4)$.

Table II. The effect of varying ε.

	ε	CPU time	#iters	Err_2	Err_∞
$Q_2(x)$	10^{-4}	8.5	5.2	1.2×10^{-3}	3.2×10^{-3}
	10^{-2}	8.2	4.2	1.2×10^{-3}	3.2×10^{-3}
	10^{-1}	8.0	3.2	2.0×10^{-3}	3.2×10^{-3}
$Q_4(x)$	10^{-4}	8.0	3.4	2.8×10^{-3}	2.6×10^{-3}
	10^{-2}	7.8	2.7	2.9×10^{-3}	2.8×10^{-3}
	10^{-1}	7.8	2.2	4.9×10^{-3}	4.4×10^{-3}

$\Delta t = 1\,\text{s}$, $n = 100$, $T_\Delta = 0.1\%$ of T_{m}.

Table III. Fachinotti: the effect of varying the time step size Δt and number of elements n.

	Δt	n	CPU time	#iters	Err_2	Err_∞
$Q_2(x)$	1	100	8.2	4.5	1.2×10^{-3}	3.2×10^{-3}
	0.25	200	34	3.1	4.1×10^{-4}	1.8×10^{-3}
	0.0625	400	151	2.5	2.1×10^{-4}	1.3×10^{-3}
$Q_4(x)$	1	100	7.9	3.1	2.7×10^{-3}	2.6×10^{-3}
	0.25	200	33	2.4	1.1×10^{-3}	1.3×10^{-3}
	0.0625	400	145	2.1	3.6×10^{-4}	6.0×10^{-4}

$T_\Delta = 0.1\%$ of T_{m}, $\varepsilon = 10^{-3}$.

a very fine grid, see Figure 8. The error in the approximated solution $\mathbf{T}$ is measured at t_{end} as

$$\text{Err}_i = \frac{\|\mathbf{T}_{\text{ref}} - \mathbf{T}\|_i}{\|\mathbf{T}_{\text{ref}}\|_i} \tag{23}$$

where the subscript i indicates the type of norm that is used.

DOI: 10.1002/nme

Table IV. Nedjar: the effect of varying the time step size Δt and number of elements n.

	Δt	n	CPU time	#iters	Err_2	Err_∞
$Q_2(x)$	1	100	8.3	14	1.4×10^{-3}	3.1×10^{-3}
	0.25	200	38	15	6.2×10^{-4}	2.3×10^{-3}
	0.0625	400	186	15	3.8×10^{-4}	1.7×10^{-3}
$Q_4(x)$	1	100	8.1	10	3.0×10^{-3}	4.0×10^{-3}
	0.25	200	35	10	1.5×10^{-3}	2.9×10^{-3}
	0.0625	400	169	11	1.0×10^{-3}	2.5×10^{-3}

Stopping criterion used is $\|\Delta T_k\|_\infty < 10^{-3}\|\Delta T_0\|_\infty$.

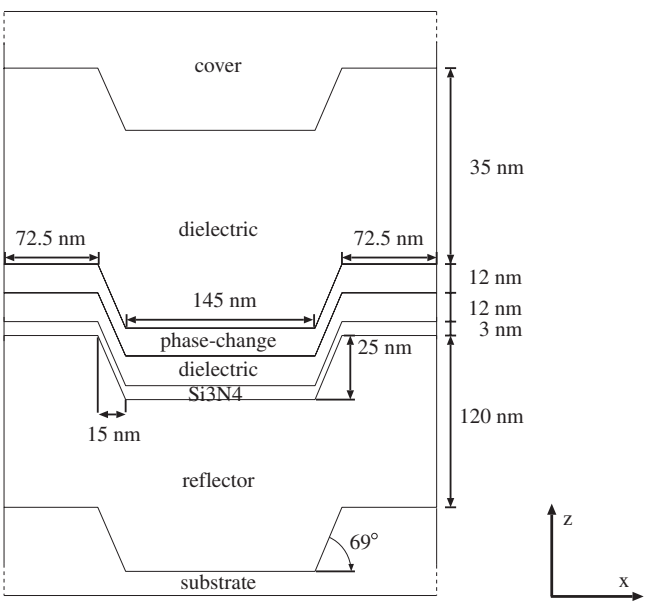

Figure 9. Cross section of the stack as used for the Blu-ray Disc simulation.

An interesting observation that can be made from Table I is that the mushy parameter T_Δ can be taken surprisingly large, without much loss of accuracy. If it is taken too small, i.e. the change in enthalpy is almost instantaneous, the computational costs increase significantly. It can be concluded that $T_\Delta = 0.1\%$ of T_m is a safe choice for most problems.

In Table II results are listed on the performance for increasing values of ε. The mushy parameter T_Δ is taken to be equal to 0.1% of T_m. From the table it follows that for values of ε smaller than 10^{-2}, the gain in accuracy becomes negligible. Therefore, a value of 10^{-3} is a safe choice for parameter ε.

Next, we choose $\varepsilon = 10^{-3}$ and $T_\Delta = 0.1\%$ of T_m and refine the spatial and the time grid simultaneously. Table III shows that the reduction in the error of the approximated solution is linear with respect to the ∞-norm and superlinear with respect to the 2-norm. The average number of

DOI: 10.1002/nme

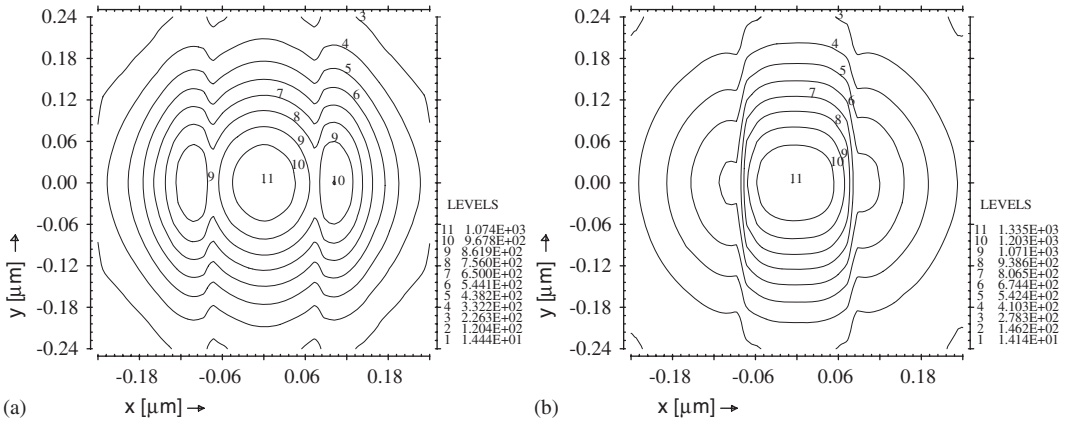

Figure 10. Temperature distributions (°C) halfway in the phase-change layer for a TM polarized spot that is incident on the center of a land and that of a groove for the Blu-ray stack of Figure 9: (a) Groove and (b) land.

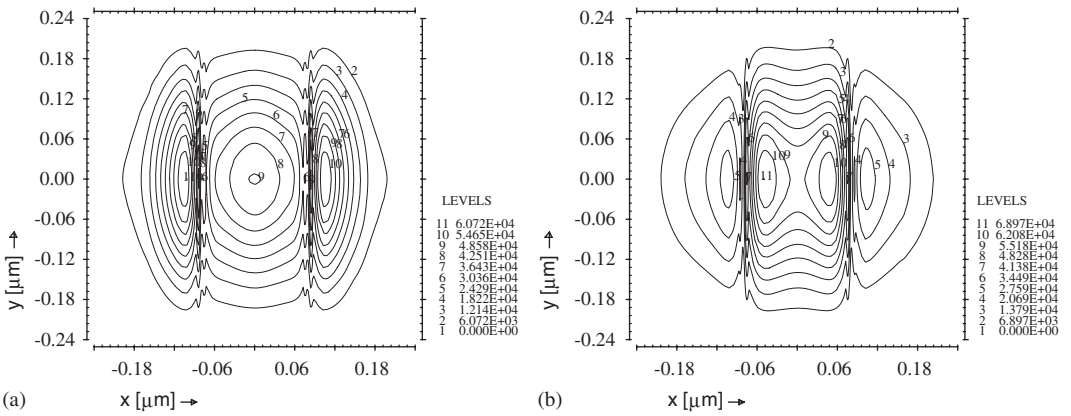

Figure 11. Absorbed energy distributions ($10^4\,\mathrm{W}/\mu\mathrm{m}^3$) halfway in the PC layer for a TM polarized spot that is incident on the grooved multilayer for the Blu-ray Disc (stack is shown in Figure 9). The NA of the lens is 0.85, the wavelength of the light is 405 nm; (a) center of the spot is in the groove and (b) center of the spot is on the land.

Newton iterations is small and almost constant for each source function. If we compare the results in Table III with those obtained using an enthalpy-based method as proposed by Nedjar [7], see Table IV; the enthalpy approach shows to be computationally more demanding and less accurate.

5. APPLICATION: BLU-RAY RECORDING SIMULATION

A typical Blu-ray recording stack is shown in Figure 9. As the name indicates, a blue laser ($\lambda = 405\,\mathrm{nm}$) is used. The land–groove structure is periodic in the radial direction of the disc.

DOI: 10.1002/nme

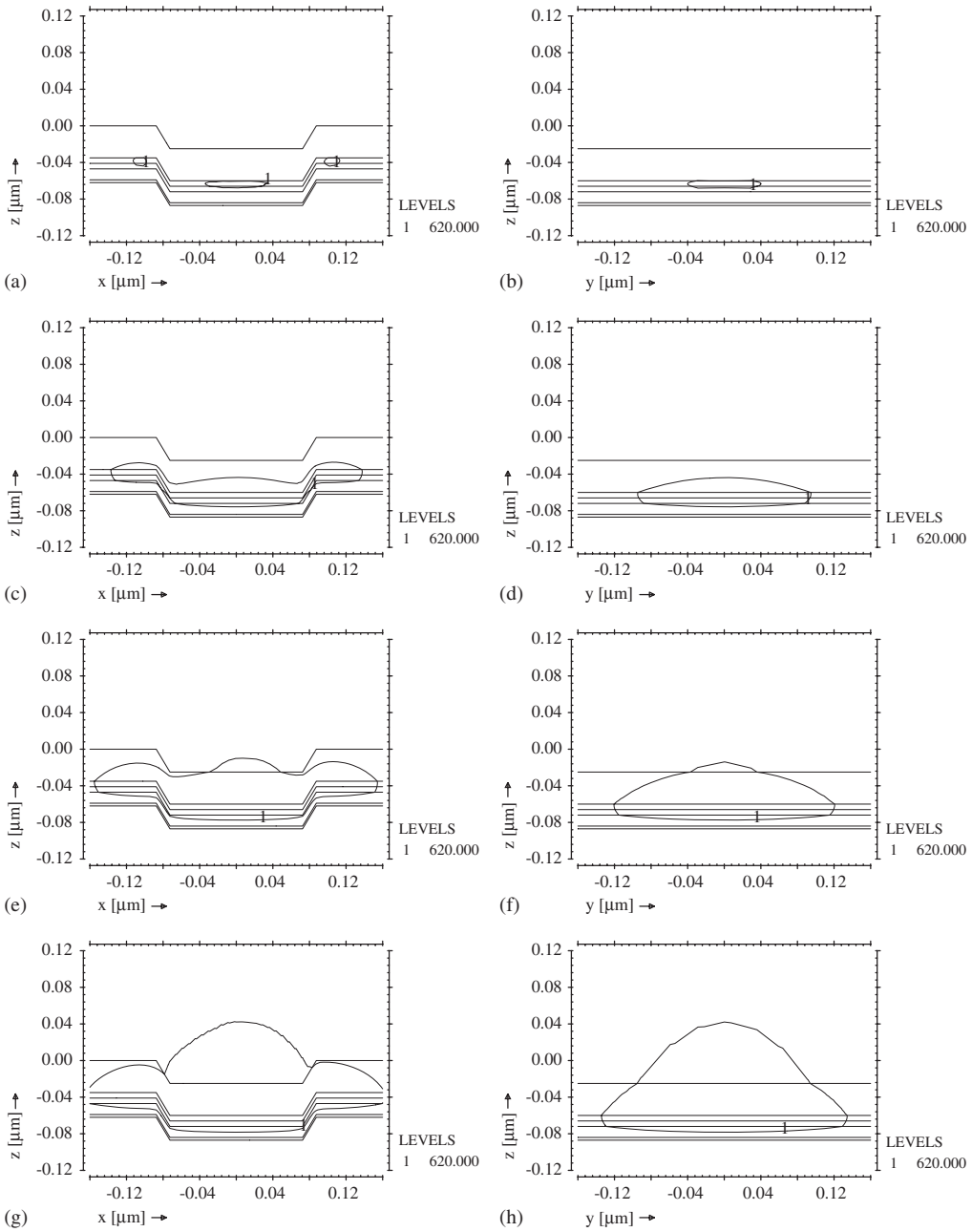

Figure 12. Evolution in time of the melting front ($T_m = 620\,^{\circ}\mathrm{C}$ contour) for a TM polarized spot that is incident on the center of a groove for the Blu-ray stack of Figure 9. The latent heat $L = 640\,\mathrm{J/cm^3}$. Intersection across the grooves (left) and along the grooves (right): (a) $t = 3\,\mathrm{ns}$; (b) $t = 3\,\mathrm{ns}$; (c) $t = 9\,\mathrm{ns}$; (d) $t = 9\,\mathrm{ns}$; (e) $t = 36\,\mathrm{ns}$; (f) $t = 36\,\mathrm{ns}$; (g) $t = 100\,\mathrm{ns}$; and (h) $t = 100\,\mathrm{ns}$.

DOI: 10.1002/nme

These grooves are needed to accurately position the optical system. If marks are recording inside a groove, the recording is called groove recording, and likewise for a land.

In the simulations, the groove depth of 50 nm has been exaggerated, to accentuate the differences between the two polarizations of the incident light. The incident field is computed with the package DIFFRACT [16] for a TE or a TM polarized Gaussian beam that is focused by a positive lens of high numerical aperture (NA = 0.85). Here, TE means that the electric field of the Gaussian beam that is incident on the lens is parallel to the grooves, and TM means that the magnetic field is parallel to the grooves. The EM field inside the disk is computed using a modified version of the optical model by Brok and Urbach [17], see Brusche *et al*. [18]. The power level of the laser is set to 15 mW, see, for instance, Meinders *et al*. [19].

Figure 10 shows the temperature distributions halfway in the phase-change layer for a TM polarized spot that is incident on the center of a land and that of a groove in case a latent heat of $640\,\mathrm{J/cm^3}$ has been taken into account. The corresponding absorbed energy distributions are shown in Figure 11.

In Figure 12 the evolution of the $T = T_\mathrm{m}$ isotherm is shown for a TM polarized spot that is incident on the center of a groove.[‡] Inside the phase-change layer, this isotherm determines the melting front. This example clearly illustrates that, in case data is recorded on both land and groove, previously written marks in adjacent tracks can be (partially) erased.

6. CONCLUSIONS

A numerical method for solving solid–liquid phase transition problems inside industrially relevant domains has been presented. The method is based on the fixed-grid temperature formulation by Fachinotti *et al*. [12]. The method is found to be efficient and accurate for Isothermal and mushy problems that are governed by boundary conditions imposed on the fixed boundaries. However, numerical complications arise in the case of isothermal problems that are governed by a heat source. These problems are resolved by introducing an artificial mushy region around the melting temperature. Finally, results have been presented for Blu-ray optical rewritable recording simulations.

ACKNOWLEDGEMENTS

The authors wish to thank the Dutch Technology Foundation (STW) for its financial support.

REFERENCES

1. Davis SH. *Theory of Solidification*. Cambridge University Press: New York, 2001.
2. Sethian JA. *Level Set Methods and Fast Marching Methods Evolving Interfaces in Computational Geometry, Fluid Mechanics, Computer Vision, and Materials Science* (2nd edn). Cambridge Monographs on Applied and Computational Mathematics 3. Cambridge University Press: Cambridge, 1999.
3. Voller VR, Swaminathan CR, Thomas BG. Fixed grid techniques for phase change problems: a review. *International Journal for Numerical Methods in Engineering* 1990; **30**(4):875–898.

[‡]In Figure 12 an additional interface is shown halfway in the phase-change layer. This interface, however, is artificial and was added for plotting purposes.

DOI: 10.1002/nme

4. Crivelli LA, Idelson SR. A temperature-based finite element solution for phase-change problems. *International Journal for Numerical Methods in Engineering* 1986; **23**(1):99–119.
5. Shamsundar N. Comparison of numerical methods for diffusion problems with moving boundaries. In *Moving Boundary Problems*, Wilson DG, Solomon AD, Boggs PT (eds). Academic Press: New York, 1978; 165–185.
6. Bhattacharya M, Basak T, Ayappa KG. A fixed-grid finite element based enthalpy formulation for generalized phase change problems: role of superficial mushy region. *International Journal of Heat and Mass Transfer* 2002; **45**(24):4881–4898.
7. Nedjar B. An enthalpy-based finite element method for nonlinear heat problems involving phase change. *Computers and Structures* 2002; **80**(1):9–21.
8. Chun CK, Park SO. A fixed-grid finite-difference method for phase-change problems. *Numerical Heat Transfer Part B* 2000; **38**(1):59–73.
9. Date AW. A strong enthalpy formulation for the Stefan problem. *International Journal of Heat and Mass Transfer* 1991; **34**(99):2231–2235.
10. Alexiades V, Solomon AD. *Mathematical Modeling of Melting and Freezing Processes*. Hemisphere: Washington, Philadelphia, London, 1993.
11. Elliott CM, Ockendon JR. *Weak and Variational Methods for Moving Boundary Problems*. Pitman: Boston, 1982.
12. Fachinotti VD, Cardano A, Huespe AE. A fast convergent and accurate temperature model for phase-change heat conduction. *International Journal for Numerical Methods in Engineering* 1999; **44**(12):1863–1884.
13. Zienkiewicz OC, Taylor RL, Zhu JZ. *The Finite Element Method*: *Its Basis and Fundamentals* (6th edn). Elsevier, Butterworth-Heinemann: Linacre House, Jordan Hill, Oxford, 2005.
14. Numerical Recipes Software. *Numerical Recipes in Fortran 77*: *The Art of Scientific Computing*. Cambridge University Press: Cambridge, 1992.
15. Peng C, Cheng L, Mansuripur M. Experimental and theoretical investigations of laser-induced crystallization and amorphization in phase-change optical recording media. *Journal of Applied Physics* 1997; **82**(9):4183–4191.
16. DIFFRACT is a product of MM Research, Inc., Tucson. Its theoretical basis has e.g. been described by M. Mansuripur. In: 'Certain computational aspects of vector diffraction problems'. *Journal of the Optical Society of America A* 1989; **6**(5):786–805.
17. Brok JM, Urbach HP. Rigorous model of the scattering of a focused spot by a grating and its application in optical recording. *Journal of the Optical Society of America A* 2003; **20**(2):256–272.
18. Brusche JH, Segal A, Urbach HP. Finite-element model for phase-change recording. *Journal of the Optical Society of America A* 2005; **22**:773–786.
19. Meinders ER, Lankhorst MHR, Borg HJ, Dekker MJ. Thermal cross-erasure issues in high-data-density phase-change recording. *Japanese Journal of Applied Physics* 2001; **40**(3):1558–1564.

DOI: 10.1002/nme